EVER
ECOLOGIC VEHICLES ● RENEWABLE ENERGIES
MONACO
March 26-29 2009

Design and Analysis of A New Outer-Rotor Permanent-Magnet Flux-Switching Machine for Electric Vehicle Propulsion

Jian-Xin Shen, Yu Wang, and Cai-Fei Wang

College of Electrical Engineering, Zhejiang University, Hangzhou, 310027, China
E-mail: j.x.shen@ieee.org

Wei-Zhong Fei, and Patrick Chi-Kwang Luk

Power and Drive Systems Group, Department of Engineering Systems and Management
Defence College of Management and Technology, Cranfield University
Shrivenham, Wiltshire, SN6 8LA, United Kingdom
E-mail: w.fei@cranfield.ac.uk

Abstract: *Permanent-magnet flux-switching (PMFS) machine is a novel doubly-salient machine which merges the advantages of both switched reluctance and permanent-magnet synchronous machines. The inherent merits such as simple structure, high torque density and high efficiency underpin PMFS machine as a potential contender for electric vehicle (EV) propulsion. However, to date, only the inner-rotor PMFS machines are widely investigated and analyzed, whilst the outer-rotor PMFS machines have hardly been addressed yet. For the most common configuration of direct drive motor, an in-wheel outer-rotor PMSF machine is proposed in this paper. The topology and operation principle of the outer-rotor configuration are introduced, and then the sizing equations are derived for the preliminary dimensions of the machine. Sequentially, a 3-phase 12/22-pole in-wheel outer-rotor PMFS machine for direct vehicle drive is designed and verified by finite element analysis (FEA). Furthermore, some techniques are employed to improve and optimize the machine performance, and the validity of the proposed techniques is demonstrated by comprehensive FEA results. Finally, based on the transient two-dimensional (2-D) FEA, the machine losses are computed and deduced, and the machine performance has been revealed.*

Keywords: Outer-rotor permanent-magnet flux-switching machines, electric vehicle propulsion, in-wheel direct drive, finite element analysis.

1. Introduction

Due to drastic issues on the protection of the environment and the shortage of fossil fuels, political and public pressures helped a lot to develop practical and efficient electric vehicles (EVs) during this decade. It is fully convinced that the zero-emission electric vehicles will be rapidly exposed on and dominate the future automotive market. The propulsion system has been one of the most essential parts in EV, direct drive EVs which are propelled by in-wheel or wheel electric machines without differential gears have drawn significant attention in both industry and academic researches. Direct drive propulsion systems can enjoy their implicit benefits such as high efficiencies, free maintenances and low noise productions in virtue of the absence of mechanical gears. Prominent features such as high torque density, excellent efficiency and terrific overload capability make permanent-

magnet (PM) brushless machine become the cogent candidate for direct drive propulsion.

The permanent-magnet flux-switching (PMFS) machine is a novel doubly-salient PM brushless machine, having both windings and magnets in the stator. The rotor is only a salient passive rotor and can be robust and fabricated at an easy rate exactly same as a switched reluctance (SR) machine. Consequently, the machine inherits the advantages of both SR machine and PM synchronous machine. Single phase PMFS machines are studied and developed as alternators in airborne application [1], motors for low energy axial fans [2] and high speed applications [3], whilst the most familiar 3-phase 12/10-pole PMFS machine was first described in [4]-[6], and further detailed investigations on this machine structure were carried out in [7]-[15]. All the aforementioned literatures have revealed that the machine has some distinct attributes of high torque density, high efficiency, excellent flux-weakening capability [16] and convenience of cooling, which are the exact stringent requirements of EV drive. When compared to conventional PM machine, due to the peculiar locations of the permanent magnets, the PMFS machine exhibits the following advantages [9]: easier to dissipate heat from the stator and therefore, to limit the temperature rise of the magnets; the influence of the armature reaction field on the working point of the magnets is almost negligible since the windings and the magnets are effectively magnetically in parallel. Consequently, the magnets demagnetization hazards owing to over load drive or over temperature are essentially prevented. Additionally, an innovative hybrid excitation flux-switching machine based on 3-phase 12/10-pole structure was presented in [17]. Moreover, 3-phase 6/4 and 6/5-pole PMFS machines for high speed operation were investigated in [18], [19].

Compared with the conventional inner-rotor machine, outer-rotor machine is intrinsically suitable for direct drive of EV as a result of its low-speed, high-torque features. So far, only the inner-rotor PMFS machines are focused in both academic researches and industry applications. The purpose of this paper is to propose and analyze a new outer-rotor PMFS machine structure especially for EVs. Firstly, the topology and operation principle of the outer-rotor PMFS machine are introduced, and the stator and rotor pole number relations defining machine phase configuration are delivered. Secondly, the sizing equations are achieved to provide simple and sufficient mean for machine's initial dimensions derivation. Finally, a 12/22-pole 3-phase in-wheel outer-rotor PMFS machine is designed, and furthermore, validated and optimized by FEA. The predicted outstanding performance implies that the proposed machine is a leading contender for direct EV drives.

2. Topology and Operation Principle

A Topology

Figure 1 (a) shows the cross-section of a typical 12/22-pole, 3-phase outer-rotor PMFS machine. As shown in the figure, the machine is composed of an inner stator that includes stator steel laminations, permanent magnets and armature coils, and an outer salient passive rotor which is exactly the same as conventional SR machine, simply constructed by stacked soft magnet steel sheets. Additionally, the concentrated windings, same as SR machine as well, are employed, which result in less copper consumption, high winding fill factor and lower copper Joule loss because of the short end windings. Compared to the conventional outer-rotor PM brushless machines having the magnets on the rotor, the magnets are inset in the middle of the stator poles, which separate the machine stator yoke. Since the magnets and coils are all placed in the stator, the major heat from the machine operation can be easily removed from the stator by various cooling methods, which is desirable for the EV applications where the ambient temperature of the machine may be high. Moreover, the number of pole-pairs in the PMFS machine is the same as the number of rotor teeth, hence, it is easy to achieve a high number of pole-pairs by employing sufficient rotor teeth. This is important for EV propulsion motors which usually require high torque and low speed.

In order to reach sufficient winding area in the outer-rotor PMFS machine, the machine main dimension configuration is proposed as $\beta_r=\beta_s=h_{pm}=h_{slot}/5$, as shown in Figure 1 (b), instead of $\beta_r=\beta_s=h_{pm}=h_{slot}$ in conventional inner-rotor PMFS machines [4]. Consequently, an adjustment of the main parameter relations to define a polyphased structure must be undertaken and can be demonstrated as follows:

$$N_r = N_s\left(2 \pm \frac{n}{2q}\right) \tag{1}$$

where N_r and N_s are machine rotor and stator pole numbers, respectively, q is the number of machine phases, and n is a natural number. The relation between the machine mechanical rotation frequency F and the electrical frequency f can be expressed as

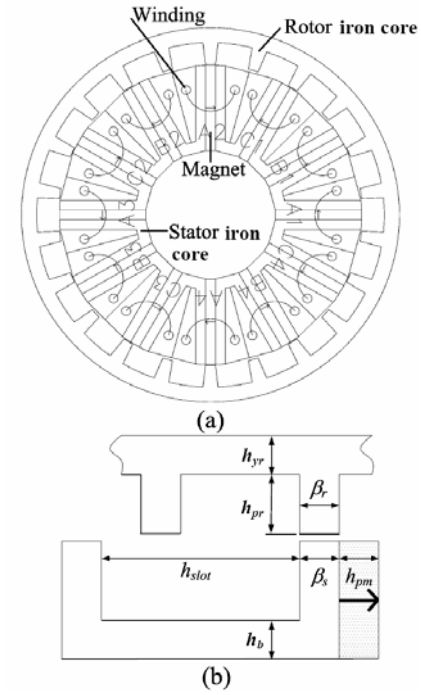

Figure 1: Topology of a 12/22-pole three-phase outer-rotor PMFS machine, (a) Cross-section. (b) Main dimension.

$$f = N_r F \tag{2}$$

By virtue of peculiar structure and zero resultant radial stress of the machine, both Nr and Ns should be even numbers. For instance, Figure 1 (a) presents a 3-phase machine with q=3, N_s=12, N_r=22, and n=1.

B Operation principle

The concept of PMFS machine was firstly introduced and investigated in [1]. The operation principle of the outer-rotor PMFS machine is illustrated as Figure 2. The PM-excited flux always exists and has a constant direction in the magnets. In Figure 2 (a), the rotor pole aligns with one of two stator teeth which are embraced by a concentrated winding coil and the PM flux which is linked in the coil goes out of the coil and into the rotor pole. When the rotor moves to the left, the rotor pole leaves the current stator pole and aligns with the next stator tooth which belongs to the same coil, as shown in Figure 2 (b), thus, the PM flux linked goes out of the rotor pole and into the stator coil. As a result, both magnitudes and polarities of the flux-linkage in the windings will vary periodically along with the rotor moves.

Figure 3 shows four typical rotor position of the 12/22-pole outer-rotor PMFS machine (shown as Figure 1 (a)) with open-circuit flux distribution. θ_r=0^o is defined at the position in Figure 3 (a) where rotor poles are fully opposite

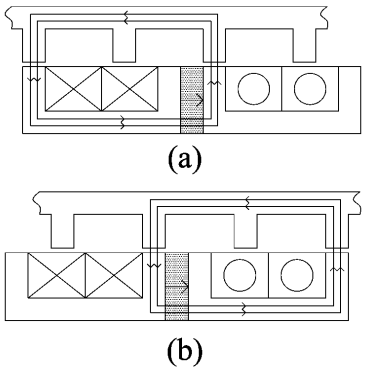

Figure 2: Operation principle of outer-rotor PMFS machine, (a) Position-a, (b) Position-b.

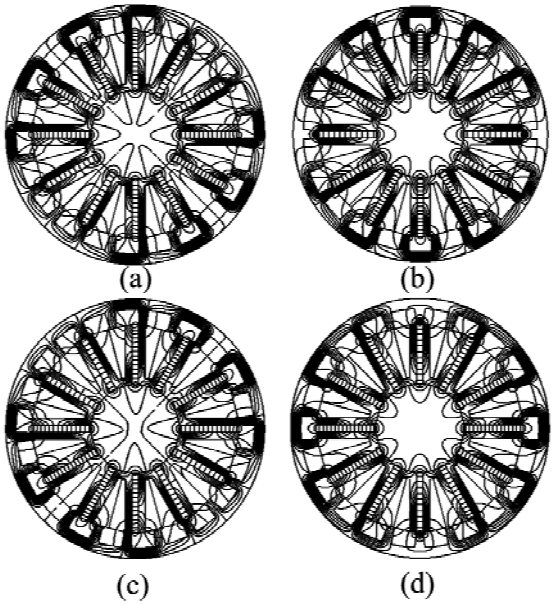

Figure 3: Four typical rotor positions of 12/22-pole three-phase outer-rotor PMFS machine with open-circuit field distributions, (a) θ_r=0^o, (b) θ_r=4.09^o, (c) θ_r=8.18^o, (d) θ_r=12.27^o.

to the respective stator teeth belonging to Phase-A. In accordance with the polarity of the magnet inset, the fluxes go into the corresponding stator teeth. Thus, the PM flux-linkage of Phase-A reaches the positive maximum when the flux going into the stator teeth is defined as positive. When the machine keeps rotating to θ_r=4.09^o anti-clockwise, Figure 3 (b), two of the rotor poles leave the corresponding stator poles belonging to Phase-A, and other two of them align with the magnets in the rest of Phase-A stator poles. Therefore, the PM flux-linkage of Phase-A reduces to zero. Likewise, as depicted in Figure 3 (c), the PM flux-linkage of Phase-A increases to the maximum again when rotor reaches θ_r=8.18^o. However, the polarity changes to negative since the fluxes go out of the stator teeth. Similar to Figure 3 (b), in the case of θ_r=12.27^o shown as Figure 3 (d), the PM flux-linkage of Phase-A reduces to zero again. If the machine keeps rotating 4.09^o forward, the rotor will return to the initial position as illustrated in

Figure 3 (a) to accomplish one electric cycle, or, 1/22 mechanical cycle. It can be noticed from the foregoing analysis that the phase PM flux-linkage in the outer-rotor PMFS machine is bipolar, which brings the machine outstanding performance.

3. Machine Modelling and Design

A Analytical Sizing Equations

Analytical sizing equations are usually helpful and necessary during the preliminary stage of machine design, which can significantly improve the machine design efficiency so as to gain the valuable competition time which is exceptionally important in industry. For outer-rotor PMFS machine, the sizing equations can be derived as follows. When the stator outer radius R_{so} is given, the stator tooth width β_s, stator magnet thickness h_{pm}, backiron thickness h_b and slot opening width h_{slot} can be given as follows:

$$\beta_s = h_{pm} = h_b = \frac{h_{slot}}{5} = \frac{\pi R_{so}}{4N_s} \tag{3}$$

Then, the area of one stator slot would be

$$A_s = R_{so}^2 \sin^2 \frac{5\pi}{8N_s} \Big/ \tan \frac{\pi}{N_s} \tag{4}$$

The electromagnetic torque T_{em} can be obtained as follows:

$$T_{em} = \frac{\frac{\pi}{16} N_r K_d K_p B_g J_{peak} R_{so}^3 l \sin^2 \frac{5\pi}{8N_s}}{\tan \frac{\pi}{N_s}} \tag{5}$$

where K_d and K_p are the leakage and winding packing factors respectively, B_g is the peak airgap flux density at no load condition, J_{peak} is the peak current density of the coils, and l is the active length of the machine. The leakage factor in outer-rotor machine is far bigger compared with the one in conventional inner-rotor machine due to its large slot opening. Inspecting equation (5), the machine torque output is proportional to R_{so}^3. R_{so} and l can be analytically gained from equation (5) during the preliminary design stage. In addition, the rotor pole height h_{pr} is chosen as 1/8 stator outer radius R_{so} and rotor yoke thickness h_{yr} is designed as twice the stator back iron thickness h_b for the sake of vibration alleviation. Hence, the machine radial dimension can be expressed as

$$R_o = \frac{9R_{so}}{8} + g + \frac{\pi R_{so}}{2N_s} \tag{6}$$

where R_o is the rotor outer radius, and g is the machine airgap.

B Machine Optimization

Machines with 5kW output at 1000rpm rated speed, which are especially suitable for urban vehicle propulsion, have been attracting tremendous attentions from both academics and industry. Since the machine is designed with three phases, the most common stator pole number 12 can be used. Higher stator pole numbers, which are not considered in this paper, are usually accompanied by higher rotor pole number that can cause higher eddy current losses and increase the assembly complexity. In this paper, a 3-phase 12/22-pole structure machine is designed and optimized for certain application. The basic machine dimensions, which is demonstrated in Table 1, can be conveniently derived from equations (3) to (6) by substituting T_{em}=50N.m, N_r=22, N_s=10, K_d=0.75, K_p=50%, B_g=2.0T, J_{peak}=7.5A/mm^2, l=50mm, and g=0.6mm into the equations.

Table 1: machine parameters.

Symbol	Machine Parameter	Value	Unit
N_s	Number of Stator Poles	12	
N_r	Number of Rotor Poles	22	
q	Number of Phases	3	
N_{coil}	Number of Winding Turns per Coil	7	
PM	PM Material	NdFe B35	
K_p	Winding Packing Factor	50%	
R_{si}	Stator Inner Radius	22.9	mm
R_{so}	Stator Outer Radius	75	mm
R_o	Rotor Outer Radius	94.8	mm
g	Air Gag	0.6	mm
h_{pr}	Rotor Pole Height	9.4	mm
β_s	Stator Tooth Width	3.8	deg
h_{pm}	PM Width	3.8	deg
β_r	Rotor tooth Width	4.9	deg
h_{ps}	Stator Tooth Width	47.2	mm
l	Machine Active Axial Length	50	mm
J_{peak}	Rated Peak Current Density	7.5	A / mm^2
U_{dc}	DC-Link Voltage	42	V
n	Rated Speed	1000	rpm
P_{em}	Rated Output Power	5.2	kW
T_{em}	Rated Output Torque	50	Nm
I_{peak}	Rated Peak Phase Current	152	A
Ψ_{pm}	Phase PM Flux Linkage	10.2	mWb
L_d	d-axis Inductance	62.7	μH
L_q	q-axis Inductance	72.0	μH
R_{ph}	Phase Resistance (100 ^{o}C)	11.1	mΩ

Comprehensive FEA are employed to validate the analytical sizing equations, determine the rest machine parameters, and optimize the machine performance. It can be facilely noticed from the FEA results that the back-EMFs of the proposed machine are essentially sinusoidal, which implies that the presented machine is congenitally suitable for BLAC operation. Consequently, the machine performance can be analyzed based on *dq*-coordinates, and the machine electromagnetic torque can be expressed as

$$T_{em} = \frac{qN_r K_p^2 A_s^2}{8}\left(\phi_{pm} + \left(\Lambda_d - \Lambda_q\right) J_d\right) J_q \qquad (7)$$

where ϕ_{pm} is the phase PM flux per turn, Λ_d and Λ_q are the *dq*- axes permeance per turn, and J_d and J_q are the *dq*-axes current density, respectively, which are restricted by

$$J_d^2 + J_q^2 = J_{peak}^2 \qquad (8)$$

Machines with various rotor pole width β_r are studied to optimize the machine back-EMF waveform [11]. In this paper, the rotor pole width is also employed to optimize the machine performance. It should be perceived that the rotor pole width after-mentioned is the normalized value β_r/β_s. Based on FEA, the phase PM flux per turn can be directly derived from open circuit field analysis and the *dq*-axes permeance per turn can be calculated by the simplified two position method [13].

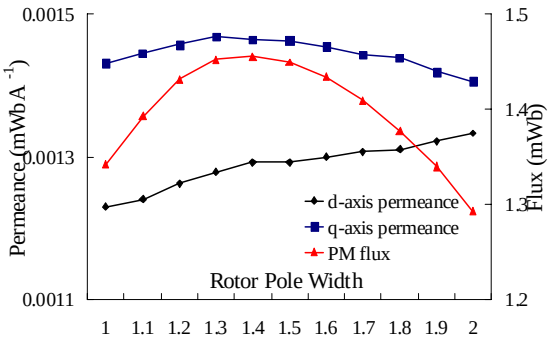

Figure 4: Variations of *dq* axes permeance per turn and phase PM flux per turn with rotor pole width.

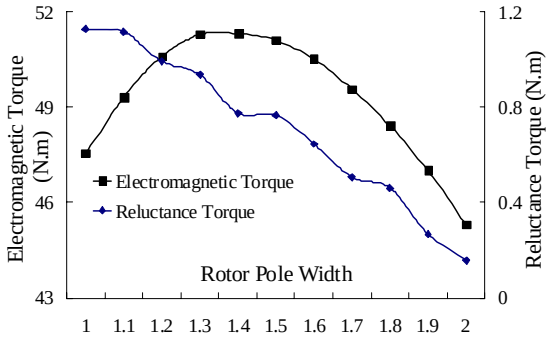

Figure 5: Variations of electromagnetic/reluctance torque with rotor pole width at rated current density.

From the FEA results as shown in Figure 4, the discrepancy between *dq*- axes permeance declines while the rotor pole width increases, as a result of machine saliency attenuation. And, the phase PM flux reaches its maximum when the rotor pole width approaches 1.4. The maximum electromagnetic torque and corresponding reluctance component at certain current density can be deduced from equations (7) and (8). Figure 5 shows the variations of electromagnetic and reluctance torque with rotor pole width at rated current density, which are calculated based on the FEA results in Figure 4. Compared to the total electromagnetic torque, the reluctance component is exiguous even negligible, and meanwhile it diminishes along with the machine rotor pole width escalation and saliency lessening. Furthermore, the electromagnetic torque which the machine could generate at rated current density, resembling the phase PM flux, achieves the maximum with the rotor pole width 1.4. Sequentially, the induced voltage (phase back-EMF) obtained for each particular rotor pole width is analyzed and the belt (nontriplen) harmonic distortion (BHD%) in the phase back-EMF is determined. There are only belt harmonics existing in the line-line back-EMF since the triplen harmonics are eradicated internally in the 3-phase machine, and the belt harmonics bring the machine torque ripple that

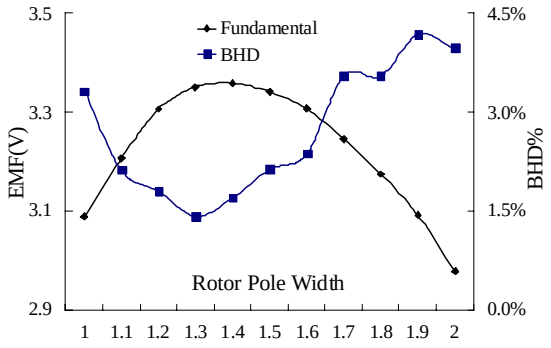

Figure 6: Variations of fundamental amplitude of phase back-EMF and belt harmonics with rotor pole width.

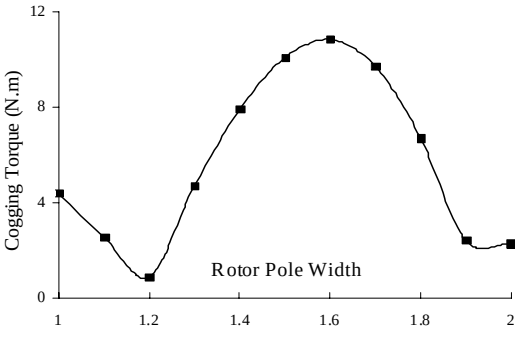

Figure 7: Variation of peak-to-peak cogging torque with rotor pole width.

would cause mechanical vibration. The fundamental amplitude of the phase back-EMF and BHD% for different rotor pole width are illustrated in Figure 6. Similar to the phase PM flux and electromagnetic torque, the fundamental amplitude of the phase back-EMF accomplishes its maximum when the rotor pole width is 1.4. However, BHD% accesses minimum with rotor pole width 1.3. Moreover, cogging torque, arising from the magnet's tendency to align itself with the minimum reluctance path given by the relative position between rotor and stator, is a parasitic source of mechanical vibration and noise which degrade machine performance, especially at low speed. It also causes startup hesitation for the motor, which is particularly undesirable for traction applications. The peak-to-peak cogging torque variation with different rotor pole width is investigated, as shown in Figure 7. The lowest cogging torque is located at where the rotor pole width is 1.2.

C Machine Parameters

According to the previous analysis, a rotor pole width 1.3 is chosen to achieve the optimal machine performance. So far only the winding turns per coil N_{coil} is still unknown, which can be calculated by the equations in [12]. The PM flux-linkage ψ_{pm} and dq-axes inductances L_d/L_q can be derived by

$$\psi_{pm} = N_{coil}\phi_{pm}, \quad L_d = N_{coil}^2\Lambda_d, \quad L_q = N_{coil}^2\Lambda_q \quad (9)$$

Furthermore, the phase resistance can be evaluated by

$$R_{ph} = \rho_{cu}\frac{4N_sN_{coil}^2\left[\left(\frac{\frac{5\pi^2}{8N_s}\sin\frac{5\pi}{8N_s}}{\sin\frac{\pi}{N_s}}+\frac{3\pi}{4N_s}\right)R_{so}+l\right]}{qk_pA_s} \quad (10)$$

The key parameters of the proposed machine are all included in Table 1, and the waveforms of phase back-EMF and cogging torque versus rotor mechanical position are both depicted in Figure 8.

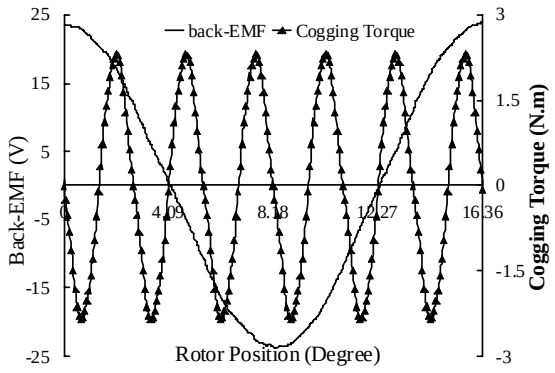

Figure 8: Phase back-EMF and cogging torque waveforms.

4. Machine Losses Analysis

Machine losses are a complex function of speed and load. Electromagnetic losses dominate the total losses in low speed machines, consequently, this paper is only concentrated on the analysis of electromagnetic losses. Electromagnetic losses can be broken down into three distinct parts, copper loss in the machine coils, core losses in the stator and rotor laminations, and eddy current losses in the permanent magnets. The motor coil copper loss can be computed from the estimated phase resistance and the torque-current profile of the machine from the FEA static analysis. The estimated resistance of one phase of the machine at 100 ^{o}C is 11.1 mΩ. Using the predicted current densities required to achieve different torque values, the copper losses for different load conditions are given in Table 2.

Transient FEA can be used to calculate the core losses in electrical steel laminations considering the harmonics. At a given frequency, the core losses for electrical steel is

$$P_c = K_hB_{\max}^2 f + K_c\left(B_{\max} f\right)^2 + K_e\left(B_{\max} f\right)^{1.5} \quad (11)$$

where K_h, K_c, and K_e are hysteresis loss, classic eddy current loss, and excess or anomalous eddy current loss coefficients, respectively, which are all information of the material from manufacturer. B_{max} is the maximum amplitude of flux density. Figure 9 shows the sensitivity of the overall lamination core losses to the machine speed and load. Increasing the load of the machine, the armature current increases the peak flux density in the lamination which leads to higher core losses. The peak load condition will approximately double the core losses compared to the no load condition. However, the core losses will not be significant compared with copper loss or eddy current losses in PM.

The magnetic field in PM will vary when the rotor rotates, since the sintered NdFeB35 has conductivity of roughly 10% that of mild steel, which can generate considerable eddy current losses. Figure 10 shows that the eddy current losses in the PM of the proposed machine are significant, which are nearly two times the copper loss under the rated load condition. Reducing eddy current losses in PM is important, not only because the magnets have a low maximum working temperature, but also

Table 2: copper loss.

Torque	Phase Peak Current	Loss
25 N.m	76 A	96 W
50 N.m	152 A	383 W
75 N.m	228 A	862 W

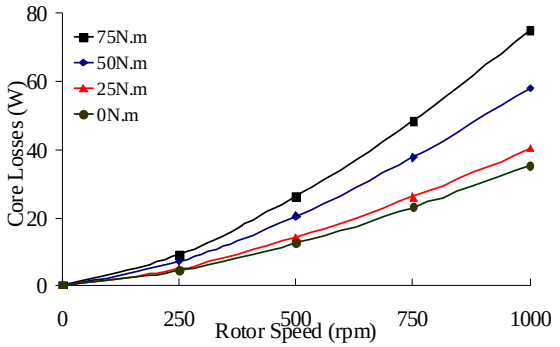

Figure 9: Core losses in stator and rotor laminations.

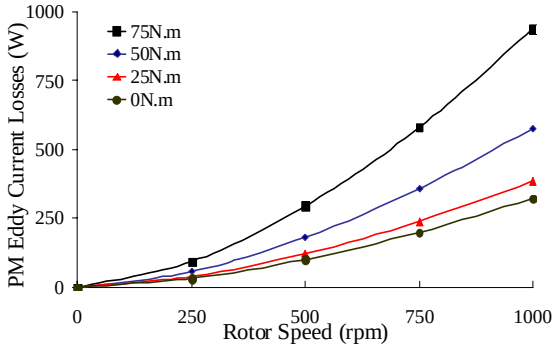

Figure 10: Eddy current losses in permanent magnets.

because the energy product of the magnets is notably condensed as their temperature increases. So researches on the PM eddy current losses as well as the means to reduce the PM eddy current losses in outer-rotor PMFS machine is especially necessary, which will be included in the authors' future paper.

From the electromagnetic loss data presented in this section, it can be found that the efficiency of the machine under rated load condition (50Nm) is just over 85%. The copper losses in winding coils and eddy current losses in PM are the major components of electromagnetic losses, which should be reduced to improve the machine efficiency. It is worth mentioning that the eddy current losses in PM grow to be the biggest part along as the operating speed increases. The eddy current losses can be effectively shrunk by segmenting the magnets into several sections, additionally the copper losses can be allayed by improve the machine winding packing factor. By the means aforementioned, the machine efficiency can overtake 90% to further confirm the proposed outer-rotor PMFS machine as a potential contender for EV propulsion.

5. Conclusion

A novel outer-rotor PMFS machine is proposed for electric vehicle propulsion in this paper. The machine topology and operation principle are introduced comprehensively, and the machine sizing equations are developed for preliminary design, which is validated by FEA. A 5kW machine is designed based on the analytical model and moreover, FEA is employed to optimize the machine performance and predict the electromagnetic losses. It is concluded that the machine possesses several distinct advantages that underpin the machine as a leading candidate for EV application, even though the machine efficiency is not as good as desired.

On the other hand, minimization techniques of the eddy current losses in permanent magnets as well as the copper loss in winding coils will be investigated in future works.

Acknowledgement

This work was supported by National Natural Science Foundation of China (NSFC, 50677061) and Qianjiang Professionals Program of Zhejiang Province (2006R10014). The work was also carried out under the collaboration MOU between Zhejiang University and Cranfield University.

References

[1] S. E. Rauch and L. J. Johnson, "Design principles of flux-switch alternators," *AIEE Trans*., vol. 74III, no. 12, pp. 1261-1269, 1955.

[2] Y. Cheng, C. Pollock, and H. Pollock, " A permanent magnet flux switching motor for low energy axial fans," in *Proc. 40th IEEE Industry Application Society Annu. Conf*., vol. 3, no. 2-6, 2005, pp. 2168-2175.

[3] Y. Chen, S. Chen, Z. Q. Zhu, D. Howe, and Y. Y. Ye, "Starting Torque of single-phase flux-switching permanent magnet motors," *IEEE Trans. Magn.*, vol. 42, no. 10, pp. 3416-3418, 2006.

[4] E. Hoang, A. H. Ben-Ahmed, and J. Lucidarme, "Switching flux permanent magnet polyphased synchronous machines," in *Proc. 7th Eur. Conf. Power Electronics and Applications*, vol. 3, 1997, pp. 903-908.

[5] E. Hoang, M. Gabsi, M. Lecrivain, and B. Multon, "Influence of magnetic losses on maximum power limits of synchronous permanent magnet drive in flux-weakening mode," in *Proc. IEEE Industry Applications Society Annu. Conf.*, vol. 1, 2000, pp. 299-303.

[6] Y. Amara, E. Hoang, M. Gabsi, and M. Lecrivain, "Design and comparison of different flux-switching synchronous machines for an aircraft oil breather application," *Euro. Trans. Electr. Power*, no. 15, pp. 497-511, 2005.

[7] W. Z. Fei and J. X. Shen, "Novel permanent magnet switching flux motors," in *Proc. 41st*

International Universities Power Engineering Conf., vol. 2, 2006, pp. 729-733.

[8] W. Hua, Z. Q. Zhu, M. Cheng, Y. Pang, and D. Howe, "Comparison of flux-switching and doubly-salient permanent magnet brushless machines," In *Proc. 8th International Conf. on Electrical machines and systems*, vol. 1, 2005, pp. 165-170.

[9] Z, Q. Zhu, Y. Pang, D. Howe, S. Iwasaki, R. Deodhar, and A. Pride, "Analysis of electromagnetic performance of flux-switching permanent magnet machines by non-linear adaptive lumped parameter magnetic circuit model," *IEEE Trans. Magn*., vol. 41, no. 11, pp. 4277-4287, 2005.

[10] Y. Pang, Z, Q. Zhu, D. Howe, S. Iwasaki, R. Deodhar, and A. Pride, "Eddy current loss in the frame of a flux-switching permanent magent machine," *IEEE Trans. Magn*., vol. 42, no. 10, pp. 3413-3415, 2006.

[11] W. Hua, M. Cheng, Z. Q. Zhu, and D. Howe, "Analysis and optimization of back-EMF waveform of a novel flux-switching permanent magnet motor," in *Proc. IEEE International Electric Machines and Drives Conf*., vol. 2, 2007, pp. 1025-1030.

[12] W. Hua, M. Cheng, Z. Q. Zhu, and D. Howe, "Design of flux-switching permanent magent machine considering the limitation of inverter and flux-weakening capability," in *Proc. 41st IEEE Industry Application Society Annu. Conf*., vol. 5, 2006, pp. 2403-2410.

[13] W. Hua and M. Cheng, "Inductance characteristics of 3-phase flux-switching permanent magent machine with doubly-salient struture," in *Proc. IEEE 5th International Power Electronics and Motion Control Conf*., vol. 3, 2006, pp. 1-5.

[14] Y. Pang, Z, Q. Zhu, D. Howe, S. Iwasaki, R. Deodhar, and A. Pride, "Comparative study of flux-switching and interior permanent magnet machines," in *Proc. 10th International Conf. on Electrical Machines and Systems*, 2007, pp. 757-762.

[15] Z, Q. Zhu, J. T. Chen, Y. Pang, D. Howe, S. Iwasaki, and R. Deodhar, "Modeling of end-effect in flux-switching permanent magnet machines," in *Proc. 10th International Conf. on Electrical Machines and Systems*, 2007, pp. 943-948.

[16] Z. W. Huang, *Research on flux-weakening capability of three-phase permanent magnet flux-switching machine*, MPhil Thesis, Zhejiang University, May 2008.

[17] E. Hoang, M. Lecrivain, and M. Gabsi, "A new structure of a switching flux synchronous polyphased machine with hybrid excitation," in *Proc. 12th Eur. Conf. Power Electronics and Applications*, 2007, pp. 1-8.

[18] W. Z. Fei and J. X. Shen, "Comparative study and optimal design of PM switching flux motors," in *Proc. 41st International Universities Power Engineering Conf.*, vol. 2, 2006, pp. 695-699.

[19] K. Wang, J. X. Shen, and S. Z. Dong, "Sensorless control and initial position estimation of permanent magnet flux switching motor," in *Proc. 10th International Conf. on Electrical Machines and Systems*, 2007, pp. 487-491.